

**NASA
Technical
Paper
3015**

November 1990

Wake Geometry Effects on Rotor Blade-Vortex Interaction Noise Directivity

R. M. Martin,
Michael A. Marcolini,
W. R. Splettstoesser,
and K.-J. Schultz

(NASA-TP-3015) WAKE GEOMETRY EFFECTS ON
ROTOR BLADE-VORTEX INTERACTION NOISE
DIRECTIVITY (NASA) 23 p CSCL 20A

N91-12315

Unclas

H1/71 0280216

NASA

NASA Technical Paper 3015

Wake Geometry Effects on Rotor Blade-Vortex Interaction Noise Directivity

**R. M. Martin, Michael A. Marcolini,
W. R. Splettstoesser, and K.-J. Schultz**

November 1990

Attached is a new copy of NASA Technical Paper 3015. The color figures were printed incorrectly in the report which was previously sent to you. Please destroy all copies of the report that you previously received.

Issued December 1990

NASA
Technical
Paper
3015

1990

Wake Geometry Effects on Rotor Blade-Vortex Interaction Noise Directivity

R. M. Martin
and Michael A. Marcolini
Langley Research Center
Hampton, Virginia

W. R. Splettstoesser
and K.-J. Schultz
Deutsche Forschungsanstalt
für Luft- und Raumfahrt
Braunschweig, West Germany

NASA

National Aeronautics and
Space Administration
Office of Management
Scientific and Technical
Information Division

Abstract

Acoustic measurements from a model rotor wind-tunnel test are presented which show that the directionality of rotor blade-vortex interaction (BVI) noise is strongly dependent on the rotor advance ratio and disk attitude. A rotor free wake analysis is used to show that the general locus of interactions on the rotor disk is also strongly dependent on advance ratio and disk attitude. A comparison of the changing directionality of the BVI noise with changes in the interaction locations shows that the strongest noise radiation occurs in the direction of motion normal to the blade span at the time of interaction for both advancing and retreating side BVI. For advancing side interactions, the BVI radiation angle down from the tip-path plane appears relatively insensitive to rotor operating condition and is typically between 40° and 55° below the disk. However, the azimuthal radiation direction shows a clear trend with descent speed, moving toward the right of the flight path with increasing descent speed. The movement of the strongest radiation direction is attributed to the movement of the interaction locations on the rotor disk with increasing descent speed.

Introduction

Helicopter blade-vortex interaction (BVI) noise is a high-amplitude, mid-frequency impulsive noise source and is due to the aerodynamic interaction of a rotor blade with the trailing vortex system generated by preceding blades. The phenomenon is created during low- and moderate-speed descent, when the rotor is flying down through its own wake. Since the interactions are highly dependent on the wake characteristics, BVI is extremely sensitive to the helicopter operating conditions. When BVI occurs, it can dominate the acoustic signal and is in the frequency range considered most important to human subjective response.

Past experimental work in rotor BVI noise has attempted to define rotor operating regimes, parametric effects, and directivity of the BVI acoustic signal from both flight measurements (refs. 1 through 3) and wind-tunnel tests (refs. 4 through 6). Early results found the BVI directivity to be generally forward of the advancing side and approximately 40° down from the rotor plane (ref. 1). Subsequent wind-tunnel programs (refs. 7 through 10) found the radiation pattern to be of dipole type, with strongest radiation in a direction 90° below the rotor plane. All these previous programs were unfortunately limited by a small number of fixed measurement locations. Most previous work has also emphasized interactions on the rotor's advancing side, although limited data showing BVI created on the retreating side have also been reported (refs. 2 and 10).

A rotor acoustics wind-tunnel test was conducted in 1986 in which measurements of a complete plane under a model rotor (refs. 11 and 12) were made.

These results show that the BVI noise source has a highly focussed directivity, but that the direction of strongest radiation can vary widely with changing advance ratio and tip-path-plane angle. The exact cause of these changes could not be established but was attributed to changing wake geometry and thus changing interaction geometry (ref. 13). Results from reference 11 also indicated that interactions in the fourth rotor quadrant have acoustic levels comparable with those from the advancing side and radiate downstream of the rotor. Due to practical constraints of wind-tunnel hardware, measurements were not acquired far enough downwind of the rotor to completely define its directivity.

A follow-on test was subsequently conducted in 1988, in which the primary objectives were (1) to establish the parametric effects on the movement of the strongest BVI acoustic radiation direction and (2) to acquire an improved spatial mapping of retreating side BVI noise directivity in the downstream direction. This paper will present some previously unpublished results from the 1986 test (ref. 11) in addition to the major results from the 1988 follow-on test.

The experiment was performed jointly with research personnel of the German Aerospace Research Establishment, the Deutsche Forschungsanstalt für Luft- und Raumfahrt (DLR), as one phase of the multiphase DLR Main Rotor/Tail Rotor Interaction Noise Program. The test was performed in the open test section of the large European aeroacoustic test facility, the Duits-Nederlandse Wind-tunnel (DNW), using a four-bladed, 40-percent dynamically scaled model of the Messerschmitt-Bölkow-Blohm (MBB) BO-105 helicopter main rotor.

An extensive range of inflow acoustic measurements was acquired in a plane underneath the rotor model with a traversing nine-microphone array. The experimental approach used in the 1988 test was quite similar to that used during the 1986 test. Details of this approach can be found in references 11 and 12.

Symbols

C_t	rotor thrust coefficient, $\frac{T}{\rho\pi\Omega^2 R^4}$
R	rotor radius, 2.0 m
r	radial distance from rotor hub to microphone, m (see fig. 1)
T	rotor thrust, N
V_z	descent speed, negative in descent, m/s
V_∞	forward speed, m/s
X	streamwise location of traversing array relative to hub, includes streamwise movement of hub due to model pitch, positive upstream, m (see fig. 1)
Y	cross-flow location of traversing array microphones relative to hub, positive towards advancing side, m (see fig. 1)
Z	vertical location of traversing array relative to hub, positive above hub, m (see fig. 1)
α_{TPP}	rotor tip-path-plane angle, positive nose up, deg (see fig. 1)
γ	descent angle, negative in descent, deg
θ	polar angle, angle from tip-path plane to microphone location, positive down, deg (see fig. 1)
μ	advance ratio, $\frac{V_\infty}{\Omega R}$
ρ	density, kg/m ³
ψ	azimuth angle in tip-path plane from rotor center to microphone location, zero over tail, 90° over rotor advancing side, deg (see fig. 1)
Ω	rotational speed of rotor, rad/sec

Abbreviations:

BVI	blade-vortex interaction
DLR	Deutsche Forschungsanstalt für Luft- und Raumfahrt (German Aerospace Research Establishment)

DNW	Duits-Nederlandse Windtunnel (German-Dutch Wind Tunnel)
MBB	Messerschmitt-Bölkow-Blohm GmbH
Mic	microphone
PaN	peak pressure of individual BVI impulse in filtered time history (500–3000 Hz), normalized by ratio of reference distance ($2R$, 4 m) to distance from microphone to assumed source position, Pa
P_{rmsN}	rms acoustic pressure in BVI spectral band (600–5000 Hz), normalized by ratio of reference distance ($2R$, 4 m) to distance from microphone to assumed source position, Pa
rms	root-mean-square quantity

Experimental Apparatus

Wind Tunnel

The test was performed in the open test section of the Duits-Nederlandse Windtunnel (DNW), located in the North East Polder, The Netherlands. The DNW is a subsonic, atmospheric, closed circuit wind tunnel with three interchangeable, closed test section configurations and one open configuration. The open configuration employs an 8×6 m nozzle that provides a free jet to the test section, which is 19 m long and surrounded by a large anechoic chamber lined with absorptive acoustic wedges. The tunnel has excellent fluid dynamic qualities even in the open throat mode (refs. 14 through 16).

Model Rotor Test Stand

The DLR rotor test stand (refs. 17 through 19) is shown installed in the DNW open test section in figure 2. For this test, the rotor test stand was housed in an acoustically insulated fiberglass shell and was attached to the computer-controlled, hydraulic sting support mechanism. The sting was covered with a streamlined sound absorptive lining to minimize acoustic reflections. Details of rotor performance and data acquisition and reduction are given in references 18 and 19 and are summarized in reference 11.

Model Rotor

The rotor is a 40-percent, dynamically scaled model of a four-bladed, hingeless BO-105 main rotor (fig. 3). The rotor has a diameter of 4 m with a root cutout of 0.350 m and a chord length of 0.121 m.

The blade cross section is an NACA 23012 airfoil, with the trailing edge modified to form a 5-mm-long tab, to match the geometry of the full-scale rotor, and a 10- by 60-mm tracking tab. The rotor blades have -8° of linear twist, a standard rectangular tip, and a solidity of 0.077. Further details are given in reference 17. The rotor blades are made of glass-fiber-reinforced plastic and have essentially the same mass and stiffness distributions as the full-scale rotor. However, the blade chord length (0.061R) is a slightly larger scale than the full-scale rotor chord (0.054R) in order to maintain Locke number scaling (ref. 17). The nominal rotor operating speed was 1050 rpm, giving an acoustic blade-passage frequency of about 70 Hz, tip speed of 218 m/s, and nominal hover tip Mach number of 0.64. The nominal rotor thrust coefficient C_t was 0.0044, or 3200 N thrust.

Acoustic Instrumentation

The acoustic instrumentation consisted of a nine-microphone inflow array mounted on a traversing system and two inflow microphones mounted on the rotor fuselage as shown in figure 2. The microphones were 1/2-in. pressure-type condenser microphones equipped with standard "bullet" nose cones. Each complete microphone system (microphone, preamplifier, and adapter) was calibrated by the electrostatic actuator method to document its frequency response. This response was flat between 5 and 5000 Hz, sufficient to capture model scale BVI noise.

Microphone calibrations were performed with a sound level calibrator at the beginning and end of the test. In addition, a pure tone calibration signal was recorded daily on all channels by signal insertion at the tape recorder inputs. The microphone signals were high-pass filtered at 4 Hz to remove very-low-frequency content associated with open jet flow "pumping."

Microphone Array Traverse System

The microphone array traverse system consisted of a horizontal wing with its span normal to the flow direction, with a total range in the flow direction of 11 m (6 m upstream, 5 m downstream) of the hub. The microphones were arranged symmetrically with respect to the tunnel centerline, spaced 540 mm apart, and nominally 2.3 m below the rotor hub. The microphone holders employed a "soft" vibration-isolating mounting. The wing and support struts were covered with an open-cell foam in an airfoil section shape. The supporting structure was covered with a 0.1-m-thick foam lining, and the base was covered with 0.8-m foam wedges. Details on control, positioning, and alignment of the array are given in reference 11.

Data Reduction and Analysis

The microphone signals and blade position reference signal (once-per-revolution signal) were synchronously digitized to provide exactly 1024 samples per rotor revolution. This digitizing was keyed by the once-per-revolution signal, and provided a sample rate of about 18 000 samples/sec, with antialiasing filters set at 9 kHz. Forty rotor revolutions of the raw acoustic signals were then digitally band-pass filtered to obtain a time series containing primarily the BVI noise content. This filtering was intended to remove the high-amplitude, low-frequency loading and thickness noise harmonics, and the high-frequency broadband noise content. The filter was an 8-pole Chebyshev filter with the passband set between 600 and 5000 Hz, the frequency range for the model BO-105 containing most of the important BVI content (ref. 20).

To calculate BVI noise directivity patterns, the rms value of 40 revolutions of the filtered acoustic signals was calculated. To remove the effect of spherical spreading decay, these rms values were normalized by the ratio of a reference distance (2 rotor radii ($2R$), 4 m) to the distance from each microphone to an assumed nominal BVI source location. Previous results using acoustic triangulation (ref. 11) have shown that the BVI noise measured on the upstream advancing side of the rotor is primarily due to interactions in the first rotor quadrant and that BVI noise measured on the downstream retreating side of the rotor is primarily due to interactions in the fourth rotor quadrant. The normalization of all the data to only a nominal advancing side, or only a retreating side, BVI source would cause an incorrect amplification in some regions of the plane. This incorrect normalization could lead to misleading interpretation or conclusions from the data. For this reason, the measurement plane was divided into two areas, each of which was normalized to either a nominal advancing or a nominal retreating side source as shown in figure 4. The specific limits of the retreating side source normalization region were defined by the results of reference 11, in which it was shown by acoustic triangulation that retreating side BVI content dominates this region. To illustrate the effect of normalizing to the two different sources, consider a measurement directly under the nominal retreating side source. The distance from the retreating side source to the measurement is 2.1 m; the distance from the advancing side source is 3.5 m. If the measurement were normalized to the advancing side source, its value would be increased by $3.5/2.1$, a factor of 1.67, over its correctly normalized value.

The effect of variation of the nominal source locations on the directivity pattern was investigated. Variation of the advancing side nominal source location from $\psi = 60^\circ$ to 80° and 60 to 90 percent radius does not have a significant effect on the location of strongest acoustic radiation, and the normalized peak rms pressure values are only affected by ± 5 percent.

The background noise levels were measured for a range of tunnel speeds and microphone array positions, with the model drive system operating at nominal rpm without the rotor blades installed. The background noise levels in the BVI spectral band were found to be at least 15 dB below the rotor BVI data; thus, no corrections have been applied.

Corrections to the measured geometric rotor shaft angle for the effect of the finite open jet potential core were calculated with the theory of reference 21. The corrected flow angle is referred to as the tip-path-plane angle, α_{TPP} .

Wake Geometry Predictions

The most recent version of the CAMRAD computer program (Comprehensive Analytical Model of Rotorcraft Aerodynamics and Dynamics (ref. 22)), now called CAMRAD/JA, was used to calculate the dynamics, aerodynamics, and wake geometry for selected test conditions presented here. The geometric, structural, and dynamic properties of the model rotor were provided by DLR and MBB and are proprietary to MBB. The code successively employs a uniform inflow model, a prescribed wake model, and a free wake model (ref. 23) to predict the rotor wake geometry with 15° azimuthal resolution. The free wake geometry (tip vortex coordinates as a function of time) was calculated for each test condition. The blade is then divided into 10 elements, and the wake geometry searched for regions where the tip vortices pass within $0.05R$ vertical distance of a blade element. Any location meeting this criterion is considered a possible blade-vortex interaction location; however, the acoustic strength of these interactions is strongly dependent on the local Mach number, the angle of intersection, the strength of the vortex, and the vertical "miss" distance from the blade.

Results

Directivity of Individual BVI Impulses

This section will present previously unpublished results from the earlier related test program (ref. 11). Reference 11 presented contours of normalized peak-to-peak BVI pressure, representing a gross measure of the BVI content. Such contours do not distinguish

between the signals generated by individual BVI's. Further research with these same results was aimed at discerning the difference in directivity of individual BVI impulses.

The filtered time histories of the data used to generate figure 7(c) of reference 11 (500–3000 Hz filter passband) show three distinctly different BVI events, called A, B, and C as shown in figure 5. The time histories were inspected to identify the peak amplitude and arrival time of each individual impulse over the entire measurement plane. Acoustic triangulation (ref. 11) was used to estimate the locations of each of the three impulses on the rotor disk. The peak amplitudes in pascals of each impulse were then normalized by the ratio of a reference distance ($2R$, 4 m) to the distance from each event's estimated location on the rotor. The resulting directivity patterns are shown in figure 6.

Impulse A (fig. 6(a)) is the earliest detectable BVI impulse, occurring at about 55° azimuth. This impulse has the lowest acoustic level and radiates a lobe at approximately 135° azimuth angle. Impulse B (fig. 6(b)), near 61° azimuth, shows higher acoustic levels and radiates more in the forward direction. Impulse C (fig. 6(c)), created at $\psi = 68^\circ$, has the highest noise levels and radiates generally forward but also somewhat toward the retreating side of the flight path. These patterns imply that the location of the noise source on the rotor disk has an important effect on the resulting directivity pattern.

Two-dimensional airfoil-vortex interaction theory has shown that this noise source has the strongest directivity within 20° of the direction normal to the blade span (ref. 24). The local Mach number and the blade-vortex intersection angle are the important parameters affecting this directionality. When an interaction is parallel, radiation is closest to normal to the span. As an interaction becomes more oblique, the radiation becomes less normal to the span. Thus the azimuthal location of the interaction, which can change both the local Mach number and intersection angle, has a major impact on the directivity pattern.

Referring again to figure 6(a), impulse A, the earliest in azimuth, is probably the most parallel, and radiates roughly normal to the $\psi = 55^\circ$ location. Impulses B and C (figs. 6(b) and (c)), occurring later in the rotation, are probably becoming less parallel, and the radiation is nearly normal but not as normal to the source azimuth as was impulse A.

Triangulation of acoustic signals to locate the BVI sources and correlation with the wake geometry of a generalized wake code implied that increasing tip-path-plane tilt (nose up) caused the interactions to move downwind on the rotor disk and thus occur at earlier azimuth angles (ref. 13). The downwind

movement of acoustic source regions was also shown by Pike (ref. 25) using a high-resolution airloads prediction code. The data presented in the next section were acquired to investigate whether such downwind movement (movement to earlier azimuth angles) of the interactions due to changing tip-path-plane angle tilt would cause a consistent change in the radiation pattern.

Directivity of Total BVI Noise as Function of Tip-Path-Plane Attitude

This section presents data acquired during the 1988 model rotor BO-105 noise test in the DNW. The BVI directivity patterns for several advance ratios were measured with changing tip-path-plane angle, as defined in table I. The most complete set of directivity patterns, acquired for an advance ratio of 0.114 for a series of 5 tip-path-plane angles, is presented in figure 7. These patterns show that the onset of BVI noise radiation occurs at $\alpha_{\text{TPP}} = 1.7^\circ$, at a moderate level (about $4 P_{\text{rmsN}}$). As α_{TPP} increases to 3.1° , the level increases to about $5 P_{\text{rmsN}}$. At $\alpha_{\text{TPP}} = 4.6^\circ$, a maximum of $5.4 P_{\text{rmsN}}$ is now seen under the advancing side, and a significant level of BVI noise is now seen downwind of the retreating side. Further increasing tip-path-plane angle to 6.1° and 7.4° shows the BVI noise radiation to be moving to the far right of the flight path. The strongest radiation lobe of the advancing side BVI content moves from directly upstream of the rotor, toward the right of the rotor (toward advancing side) and downwind as the tip-path-plane angle increases.

This general trend was consistently measured for a range of moderate flight speeds at advance ratios from 0.090 to 0.250. (Refer to table I.) A second example for an advance ratio of 0.150 is shown in figure 8. The BVI lobe from the advancing side interactions starts with a moderate level upstream of the rotor, and as tip-path-plane angle increases, the lobe moves to the right of the flight path and the acoustic levels increase. The lobe finally moves off of the measurement plane at $\alpha_{\text{TPP}} = 6.5^\circ$. The repeatability of the noise patterns measured at similar conditions during the 1986 and 1988 tests is quite good. The $\alpha_{\text{TPP}} = 3.1^\circ$ pattern of figure 7(b) can be compared with figure 7(c) of reference 11; the $\alpha_{\text{TPP}} = 0.6^\circ$ pattern of figure 8(a) can be compared with figure 7(e) of reference 11. Absolute levels cannot be compared between the two data sets as reference 11 presents peak-to-peak pressures rather than rms pressures.

One aim of the present test was to acquire directivity data on retreating side BVI at locations farther downstream than the earlier test (ref. 11). Unfortunately the results given here show that the measurement locations were still not far enough downwind to

completely define the retreating side BVI radiation lobe. The maximum downwind location of the microphone array was limited by interference with the sting and by the increasing proximity to the lower shear layer of the open jet test section. However, the patterns for $\mu = 0.114$ and 0.150 both indicate that the retreating side downwind lobe moves from under the aft retreating quadrant towards the flight path (or towards the right of the noise pattern) with increasing tip-path-plane angle. The levels of the retreating side BVI seem to be comparable in magnitude with that radiated from the advancing side. Retreating side BVI lobes are evident in the patterns of the remaining test conditions but are not sufficiently defined to make more specific conclusions.

Prediction of Possible BVI Locations From a Free Wake Analysis

The wake geometry predictions from the Scully free wake in CAMRAD/JA were used to estimate the most likely BVI regions on the rotor disk, as explained in the section "Wake Geometry Predictions." The results for three of the five tip-path-plane angles at $\mu = 0.150$ shown in figure 8 are given in figure 9. The specific contour values have been removed from figure 9 for clarity; the reader may obtain these values from figure 8.

The predicted BVI locations are shown in these figures by the symbols, with different symbols used to differentiate between each of the four blades' tip vortices. The wake geometry is not a single time prediction; it represents all possible interactions of one blade with the four tip vortices as the blade moves through one revolution. The sizes of the symbols are scaled with each vortex's vertical "miss distance," with the largest symbols being the closest interactions. The open symbols signify that the vortex passed below the blade, the solid symbols signify that the vortex passed above the blade. A cross centered in an open symbol signifies the vortex was very close to the blade.

Figure 9(a) presents the interaction regions and the BVI directivity pattern for $\mu = 0.150$ and $\alpha_{\text{TPP}} = 0.6^\circ$. The region of strongest BVI on the rotor disk is located between $\psi = 80^\circ$ and 90° , 30 and 80 percent radius. The strongest acoustic levels are probably generated from vortex 1 (circular symbols), where it passes from above to below the blades at about $\psi = 90^\circ$, 50 percent radius. (Results of reference 26 indicate that the passage of a vortex through the disk was most likely to generate a strong impulsive signal). The direction of strongest acoustic radiation is roughly normal to $\psi = 80^\circ$.

Three very close interactions are indicated on the retreating side, between $\psi = 270^\circ$ and 330° in

the inboard area: vortex 2 (squares) at $\psi = 270^\circ$, 50 percent radius; vortex 2 at $\psi = 270^\circ$, 25 percent radius; and vortex 1 (circles) at $\psi = 320^\circ$, 40 percent radius. Little acoustic radiation from the retreating side was measured; this is to be expected as the local Mach number at these inboard locations is quite low.

At $\alpha_{\text{TPP}} = 3.6^\circ$ (fig. 9(b)), the primary advancing side interactions are probably due to vortex 1 (circles), vortex 3 (diamonds), and vortex 4 (triangles), all near the line at $\psi = 60^\circ$. Vortex 4 is passing from above to below the blades when it is near $\psi = 60^\circ$, 80 percent radius. The primary acoustic radiation direction has moved considerably to the right of the flight path for this flight condition, and now is roughly normal to the line at $\psi = 50^\circ$ or 60° . The increased acoustic levels may be due to the fact that the interactions are occurring nearer the tip than at $\alpha_{\text{TPP}} = 0.6^\circ$ with a higher local Mach number.

The strongest retreating side BVI is due to vortex 1 (circles), near $\psi = 300^\circ$, 80 percent radius. Moderate BVI acoustic levels are measured below the aft retreating side of the rotor, in a direction approximately normal to $\psi = 300^\circ$.

Finally, at $\alpha_{\text{TPP}} = 6.5^\circ$ (fig. 9(c)), only one close BVI is predicted (vortex 1, circles) on the rotor, near $\psi = 40^\circ$, 90 percent radius. The acoustic levels have also decreased from their previous levels, to be expected since the local Mach number of such an interaction is lower than the later azimuth angles. The strongest radiation lobe has moved even farther downstream and to the right of the flight path, again in a direction roughly perpendicular to the BVI azimuthal location.

Very little retreating side interaction activity is predicted, which matches well with the negligible BVI acoustic levels measured below the retreating side.

The free wake calculations were used to estimate the interaction locations for test conditions at several other advance ratios, with consistent correlation between the general azimuthal location of the strongest interactions and the general direction of the strongest acoustic radiation. The wake geometry results show that increasing rotor disk angle causes the general region of BVI to move downstream on the rotor disk, causing the interactions to occur at earlier azimuth angles, and therefore causing the noise to radiate more to the right and downstream of the rotor flight path. The comparison of the BVI location regions with the acoustic directivity patterns clearly support the conclusion that the BVI noise source radiates most strongly in a direction roughly normal to the blade span.

Trend of Direction of Strongest BVI With Flight Condition

The locations of strongest radiation, in terms of polar angle θ (angle down from the rotor) and azimuthal angle ψ (angle in the rotor plane), are given in table I. For each advance ratio, the maximum normalized BVI rms levels are quite close, ranging from 5.4 to 6.7 $P_{\text{rms}}N$. However, the location of the maximum varies widely. The earlier directivity results of reference 11 for six high BVI noise conditions indicated that the highest BVI noise levels are generated at moderate advance ratios ($\mu = 0.116$ to 0.146) and that lower levels are generated at lower and higher advance ratios. The more recent results presented here show that strong BVI levels are generated over a much wider range of advance ratio and tip-path-plane angle and that the location of the strongest radiation region varies considerably.

To investigate the movement of the strongest BVI lobe, the polar angle θ and azimuth angle ψ of strongest BVI radiation direction are plotted versus descent angle and vertical descent speed in figures 10 and 11. Descent angle and speed are both defined negative for descending flight. The polar angle appears fairly insensitive to descent angle, always in the range of 40° to 55° down from the disk (fig. 10(a)). A weak trend of increasing polar angle with increasing (more negative) descent speed is seen (fig. 10(b)).

The plot of azimuth angle versus descent angle (fig. 11(a)) shows a clear trend of decreasing azimuth angle with increasing descent. The plot of azimuth angle versus descent speed (fig. 11(b)) collapses to a single curve. The results show that at any forward speed, control of the descent speed will control the azimuthal angle of highest BVI noise radiation. In slow descent (for example, -1 m/s), the BVI noise radiates directly upstream. Higher values of descent speed (for example, -5 m/s) cause the BVI noise to radiate more to the right of the flight path of the rotor. The results clearly show that operational considerations can control the direction of BVI noise radiation.

Conclusions

Acoustic measurements from a model rotor wind-tunnel test are presented which show that the directionality of mid-frequency rotor blade-vortex interaction (BVI) noise is strongly dependent on the rotor advance ratio and disk attitude. A rotor free wake analysis is used to show that the general locus of interactions on the rotor disk is also strongly dependent on advance ratio and disk attitude (tip-path-plane angle). A comparison of the changing directionality of the BVI noise with changes in the interaction locations shows that the strongest noise radiation occurs

in a direction normal to the blade azimuth at the time of interaction. At low tip-path-plane angles most advancing side interactions occur at azimuths between 70° and 90° , and the BVI noise radiates directly upstream of the rotor advancing side. As tip-path-plane angle increases, the interactions occur at earlier azimuth angles and, thus, radiate more to the right of the flight path. At large tip-path-plane angles, the interactions occur as early as an azimuth angle of 30° , and the BVI noise radiates more to the advancing side and downwind of the rotor flight path.

The noise radiation from the retreating side interactions was also found to vary consistently with rotor angle. The retreating side radiation lobe tends to move from directly downstream of the retreating side towards the flight path centerline with increasing tip-path-plane angle. This is attributed to the

movement of the retreating side interactions at azimuth angles from roughly 270° to near 330° with increasing tip-path-plane angle.

The BVI radiation angle down from the tip-path plane (polar angle) appears relatively insensitive to rotor operating condition, typically between 40° and 55° down from the disk. The BVI radiation angle in the tip-path plane (azimuthal angle) shows a clear trend with descent angle and descent speed. The best correlation was found between azimuth angle and rotor descent speed, with azimuth angle decreasing with increasing descent speed.

NASA Langley Research Center
Hampton, VA 23665-5225
August 31, 1990

References

1. Boxwell, D. A.; and Schmitz, F. H.: Full-Scale Measurements of Blade-Vortex Interaction Noise. Preprint No. 80-61, 36th Annual Forum Proceedings, American Helicopter Soc., Inc., May 1980.
2. Charles, Bruce D.: Acoustic Effects of Rotor-Wake Interaction During Low-Power Descent. *National Symposium on Helicopter Aerodynamic Efficiency*, American Helicopter Soc., Inc., 1975, pp. 7-1-7-8.
3. Tangler, James L.: Schlieren and Noise Studies of Rotors in Forward Flight. *33rd Annual National Forum*, American Helicopter Soc., Inc., May 1977, pp. 77.33-05-1-77.33-05-12.
4. Spletstoesser, W. R.; Schultz, K. J.; Boxwell, D. A.; and Schmitz, F. H.: *Helicopter Model Rotor-Blade Vortex Interaction Impulsive Noise: Scalability and Parametric Variations*. NASA TM-86007, TM-84-A-7, 1984.
5. Hoad, Danny R.: Helicopter Model Scale Results of Blade-Vortex Interaction Impulsive Noise as Affected by Tip Modification. *36th Annual Forum Proceedings*, American Helicopter Soc., Inc., May 1980, pp. 80-62-1-80-62-13.
6. Martin, R. M.; and Connor, Andrew B.: *Wind-Tunnel Acoustic Results of Two Rotor Models With Several Tip Designs*. NASA TM-87698, 1986.
7. Schlinker, Robert H.; and Amiet, Roy K.: *Rotor-Vortex Interaction Noise*. NASA CR-3744, 1983.
8. Ahmadi, Ali R.: *An Experimental Investigation of the Chopping of Helicopter Main Rotor Tip Vortices by the Tail Rotor*. NASA CR-177338, 1984.
9. Hubbard, J. E., Jr.; and Harris, W. L.: Model Helicopter Rotor Impulsive Noise. *J. Sound & Vibration*, vol. 78, no. 3, Oct. 8, 1981, pp. 425-437.
10. Leighton, Kenneth P.; and Harris, Wesley L.: *On Mach Number Scaling of Blade/Vortex Noise Produced by Model Helicopter Rotors at Moderate Tip Speeds*. FDRL Rep. 84-3, Dep. of Aeronautics and Astronautics, Massachusetts Inst. of Technology, Oct. 1984.
11. Martin, R. M.; Spletstoesser, W. R.; Elliott, J. W.; and Schultz, K.-J.: *Advancing-Side Directivity and Retreating-Side Interactions of Model Rotor Blade-Vortex Interaction Noise*. NASA TP-2784, AVSCOM TR 87-B-3, 1988.
12. Martin, R. M.; Spletstoesser, W. R.; Elliott, J. W.; and Schultz, K.-J.: *Acoustic Measurements From a Rotor Blade-Vortex Interaction Noise Experiment in the German-Dutch Wind Tunnel (DNW)*. NASA TM-4024, AVSCOM TR 87-B-4, 1988.
13. Spletstoesser, W. R.; Schultz, K. J.; and Martin, Ruth M.: Rotor Blade-Vortex Interaction Impulsive Noise Source Identification and Correlation With Rotor Wake Predictions. AIAA-87-2744, Oct. 1987.
14. Van Ditschuijzen, J. C. A.; Courage, G. D.; Ross, R.; and Schultz, K.-J.: Acoustic Capabilities of the German-Dutch Wind Tunnel DNW. AIAA-83-0146, Jan. 1983.
15. *Compilation of Calibration Data of the German-Dutch Wind Tunnel*. MP-82.01, DNW, Mar. 13, 1982.
16. Ross, R.; Van Nunen, J. W. G.; Young, K. J.; Allen, R. M.; Van Ditschuijzen, J. C. A.: *Aero-Acoustic Calibration of DNW Open Jet*. DNW TR 82.03, Boeing Doc. D6-51501, July 1982.
17. Langer, H. J. (SCITRAN, transl.): *DFVLR Rotorcraft—Construction and Engineering*. NASA TM-77740, 1984.
18. Langer, H.-J. (Leo Kanner Assoc., transl.): *Data Input, Processing and Presentation*. NASA TM-77739, 1984.
19. Breustedt, Wolfgang (SCITRAN, transl.): *Data Analysis on the Rotor Test Stand Program for Interactive Processing*. NASA TM-77948, 1985.
20. Burley, Casey L.; and Martin, Ruth M.: Tip-Path-Plane Angle Effects on Rotor Blade-Vortex Interaction Noise Levels and Directivity. *44th Annual Forum Proceedings*, American Helicopter Soc., Inc., c.1988, pp. 757-771.
21. Heyson, Harry H.: *Use of Superposition in Digital Computers To Obtain Wind-Tunnel Interference Factors for Arbitrary Configurations, With Particular Reference to V/STOL Models*. NASA TR R-302, 1969.
22. Johnson, Wayne: *A Comprehensive Analytical Model of Rotorcraft Aerodynamics and Dynamics. Part I: Analysis Development*. NASA TM-81182, USAAVRADCOM TR-80-A-5, 1980.
23. Scully, M. P.: *Computation of Helicopter Rotor Wake Geometry and Its Influence on Rotor Harmonic Airloads*. ASRL TR 178-1 (Contracts N00019-73-C-0378 and N00019-74-C-0321), Massachusetts Inst. of Technology, Mar. 1975.
24. Widnall, Sheila: Helicopter Noise Due to Blade-Vortex Interaction. *J. Acoust. Soc. America*, vol. 50, no. 1, pt. 2, July 1971, pp. 354-365.
25. Pike, A. C.: Application of High Resolution Airload Calculations to Helicopter Noise Prediction. Paper presented at the AHS National Specialists' Meeting on Aerodynamics and Aeroacoustics (Arlington, Texas), Feb. 25-27, 1987.
26. Hoad, Danny R.: *Helicopter Blade-Vortex Interaction Locations—Scale-Model Acoustics and Free-Wake Analysis Results*. NASA TP-2658, AVSCOM TM 87-B-1, 1987.

Table I. Maximum BVI Noise Values and Directions of Maxima

μ	α_{TPP} , deg	Descent angle, γ , deg	Descent speed, V_z , m/s	Maximum PrmsN, Pa	Polar angle, θ , deg	Azimuthal angle, ψ , deg
0.090	-1.1	0.3	0.1	2.0	47.4	163.3
0.090	1.9	-2.7	-0.9	2.3	51.8	189.5
0.088	4.9	-5.7	-1.9	4.3	46.4	185.7
0.088	7.9	-8.7	-2.9	5.6	41.9	144.5
0.114	1.7	-3.0	-1.3	4.0	40.7	166.0
0.114	3.1	-4.4	-1.9	5.1	44.6	148.0
0.113	4.6	-5.9	-2.6	5.4	39.2	129.8
0.113	6.1	-7.4	-3.2	5.2	41.7	110.6
0.112	7.4	-8.6	-3.7	5.2	46.8	101.3
0.135	0.9	-2.7	-1.4	3.9	39.2	140.2
0.135	2.4	-4.2	-2.2	5.8	41.9	125.5
0.135	3.9	-5.7	-3.0	6.0	43.0	116.6
0.133	5.4	-7.2	-3.7	5.2	47.5	73.3
0.133	6.9	-8.6	-4.4	4.5	49.4	63.4
0.151	0.6	-2.9	-1.7	4.5	39.2	140.2
0.150	2.1	-4.3	-2.5	5.8	46.4	95.7
0.150	3.6	-5.8	-3.4	6.7	46.4	95.7
0.149	5.0	-7.2	-4.2	6.1	48.3	68.2
0.149	6.5	-8.7	-5.0	4.5	49.4	63.4
0.181	-0.4	-3.0	-2.1	3.6	40.1	119.7
0.180	2.6	-5.8	-4.1	6.0	53.2	51.3
0.180	5.6	-8.8	-6.2	6.1	50.6	59.0
0.249	-3.3	-2.9	-2.8	3.5	55.9	45.0
0.250	-0.3	-5.9	-5.7	6.0	48.0	41.2
0.293	-9.0	0.4	0.5	2.5	67.7	189.9
0.296	-6.0	-2.8	-3.1	3.8	54.6	48.0
0.298	-3.0	-5.9	-6.8	6.7	53.2	51.3

Page intentionally left blank

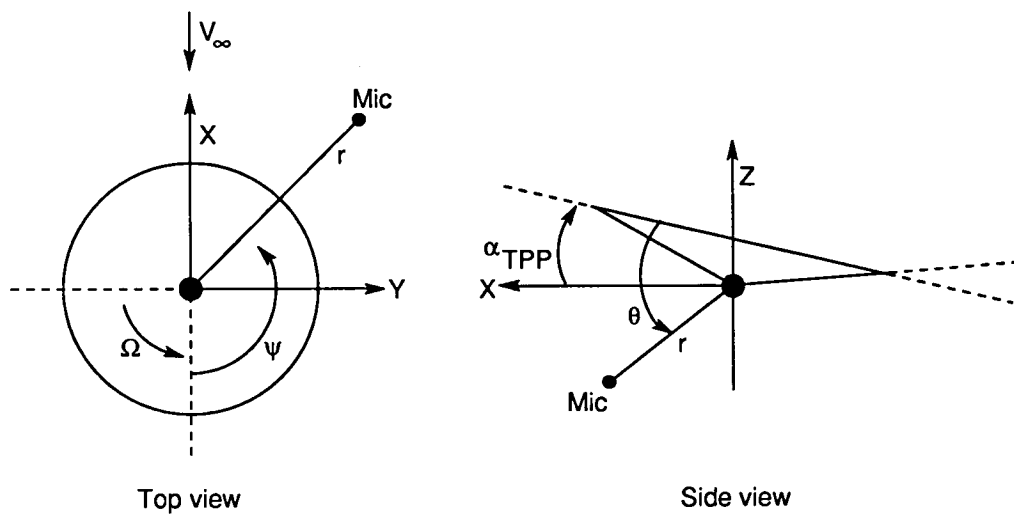
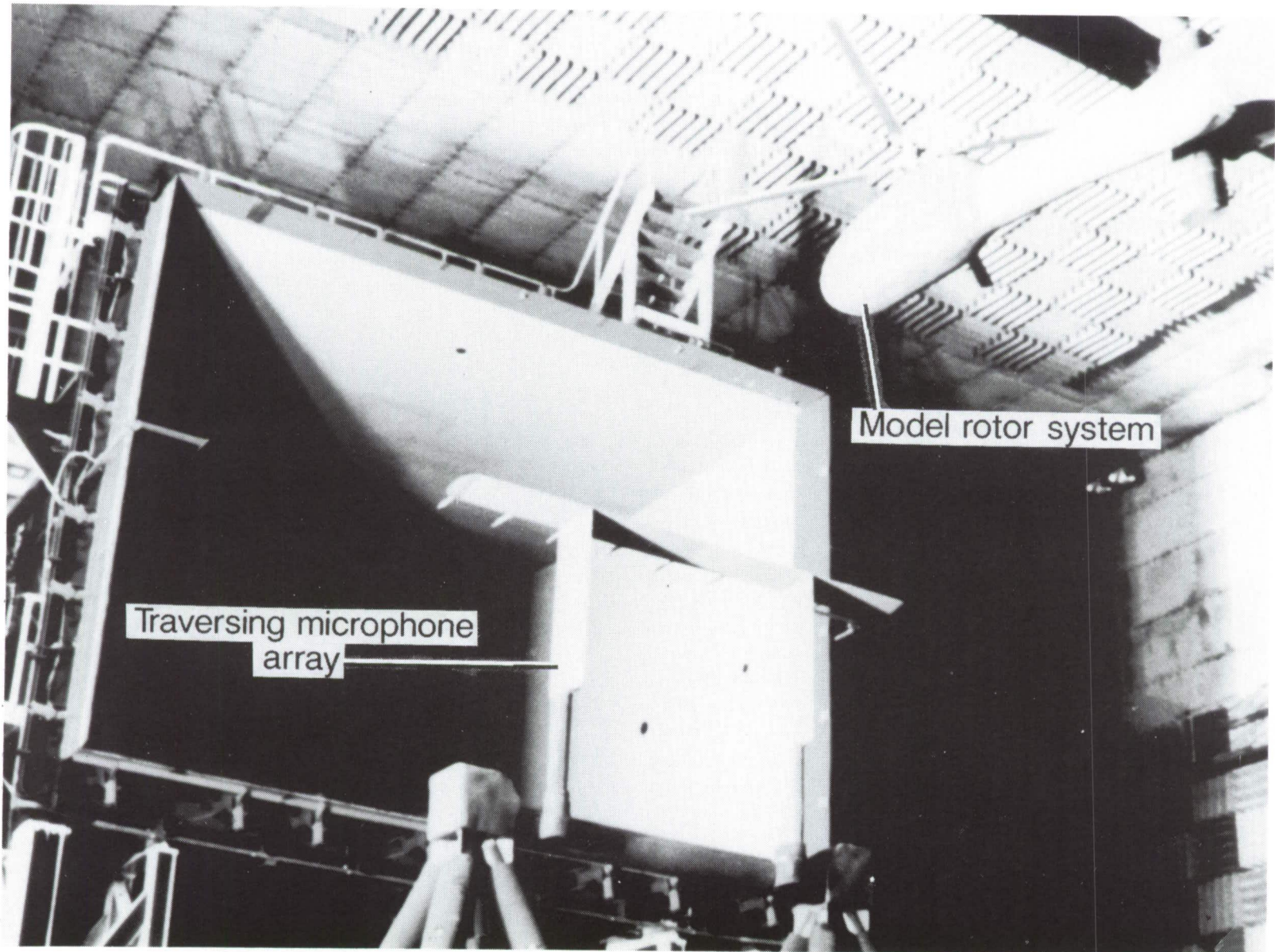


Figure 1. Geometry of coordinate system.



L-90-43

Figure 2. DLR rotor test stand and traversing microphone array in DNW open test section.

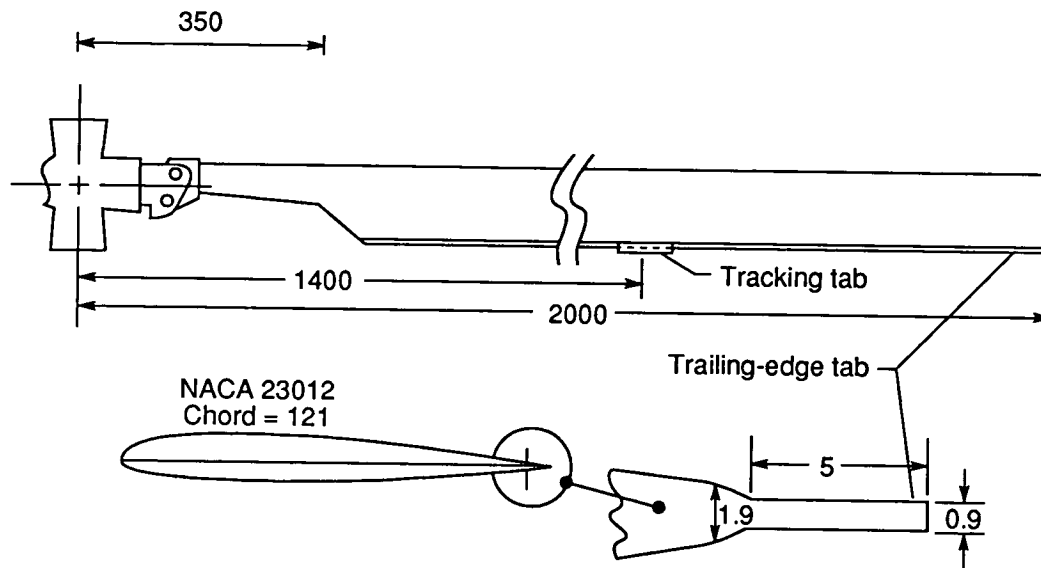


Figure 3. Geometry of model BO-105 rotor. Dimensions are in millimeters.

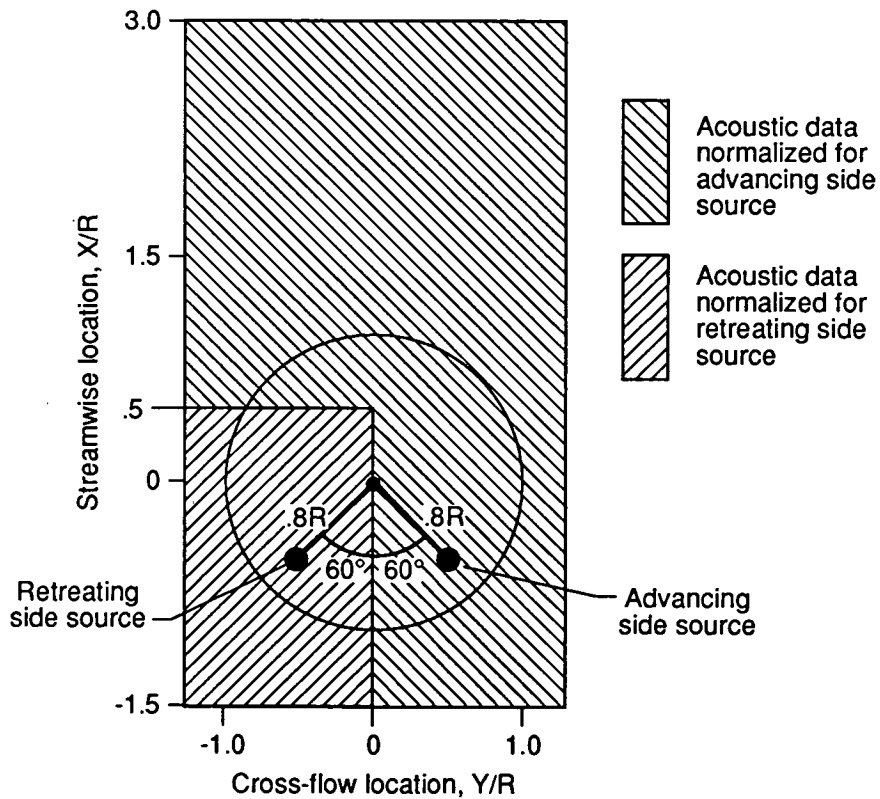


Figure 4. Normalization regions and source locations for spherical spreading correction.

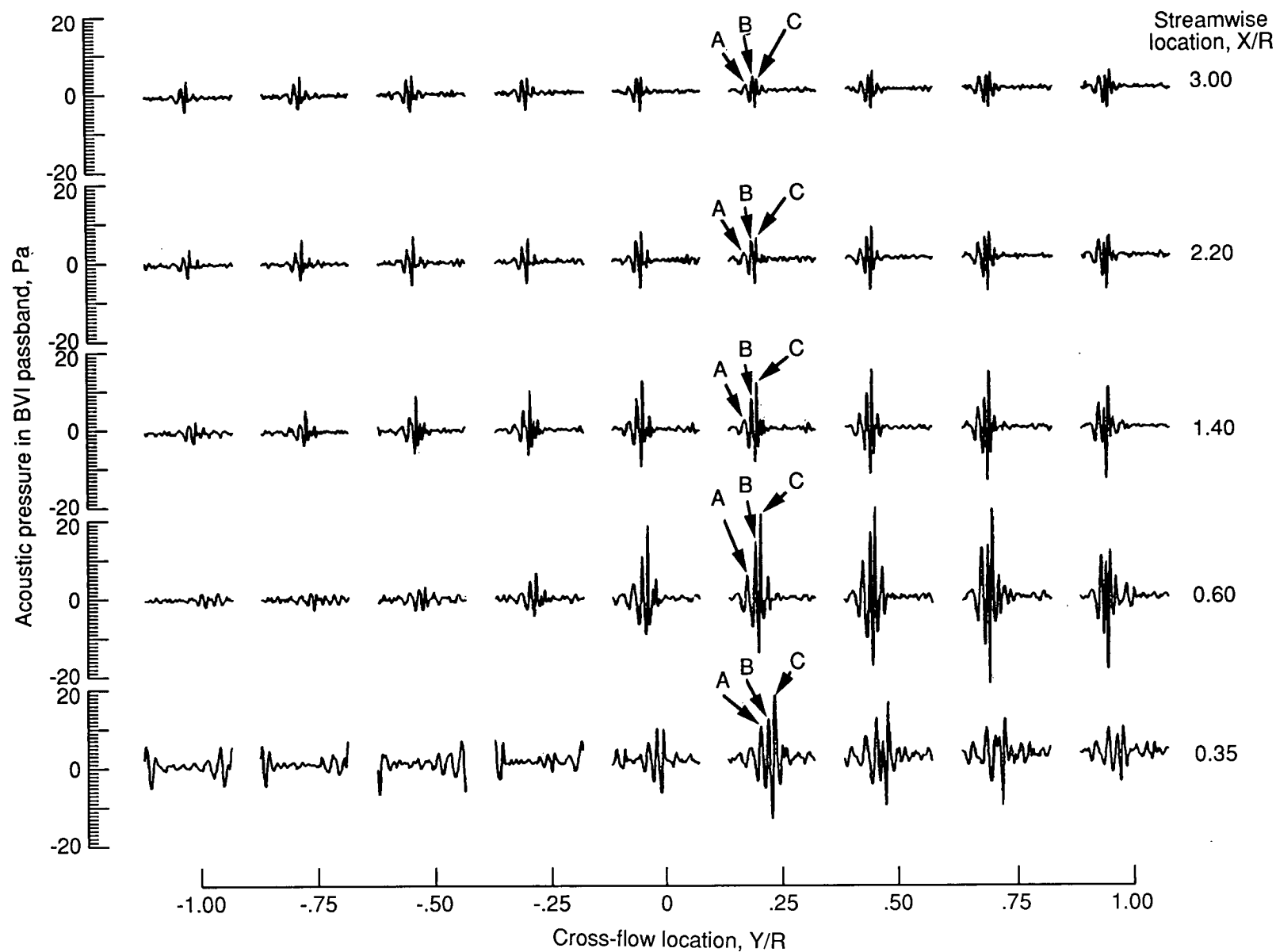
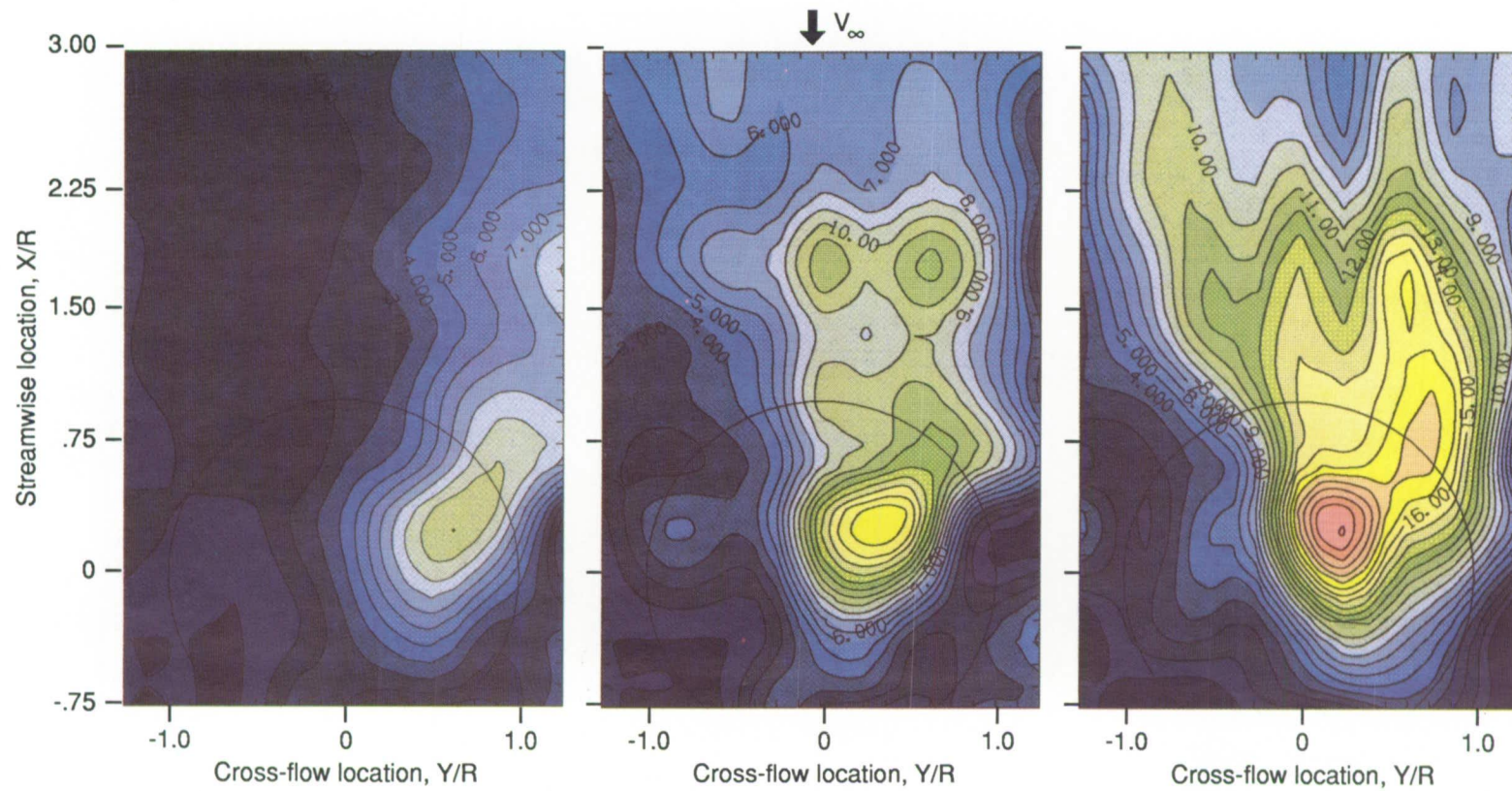


Figure 5. Filtered time histories (500 to 3000 Hz passband) showing multiple impulses.



(a) Impulse A; $r/R = 0.67$; $\psi = 55^\circ$. (b) Impulse B; $r/R = 0.83$; $\psi = 61^\circ$. (c) Impulse C; $r/R = 0.88$; $\psi = 68^\circ$.

Figure 6. Directivity of peak value of filtered time histories for impulses A, B, and C (each pattern normalized for spherical spreading from each impulse source location), PaN, for $\mu = 0.116$ and $\alpha_{TPP} = 3.0^\circ$.

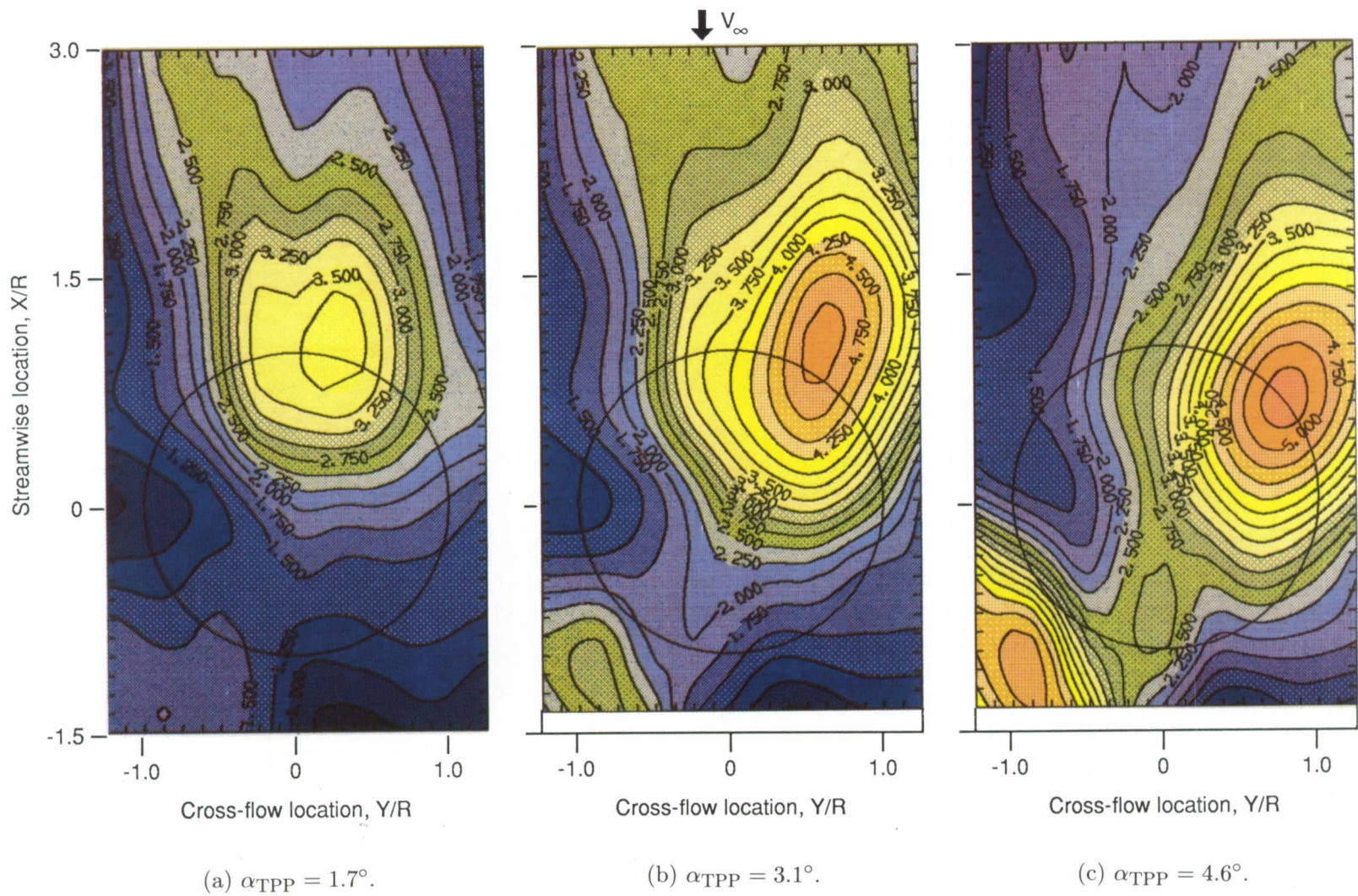
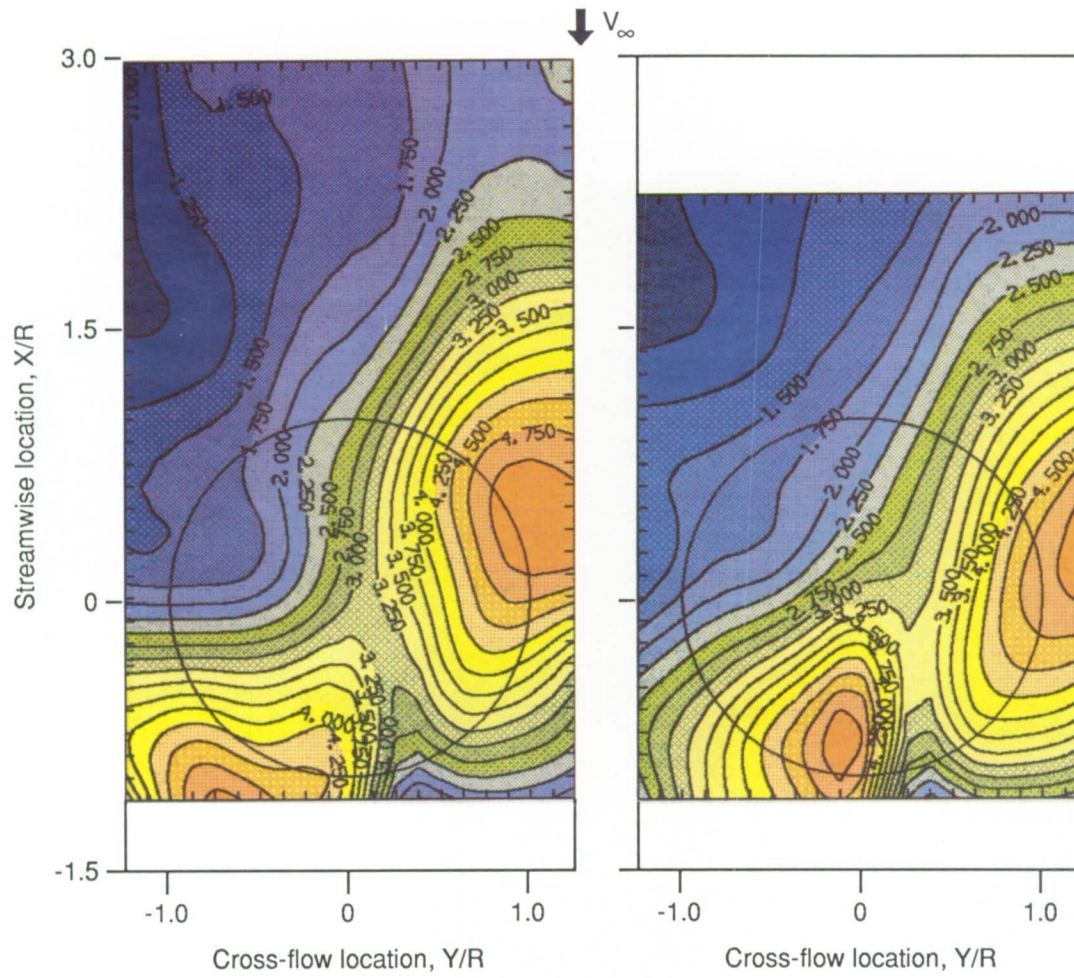


Figure 7. Directivity of rms of filtered time histories (normalized for spherical spreading as shown in fig. 4), $P_{\text{rms}N}$, for $\mu = 0.114$.



(d) $\alpha_{\text{TPP}} = 6.1^\circ$.

(e) $\alpha_{\text{TPP}} = 7.4^\circ$.

Figure 7. Concluded.

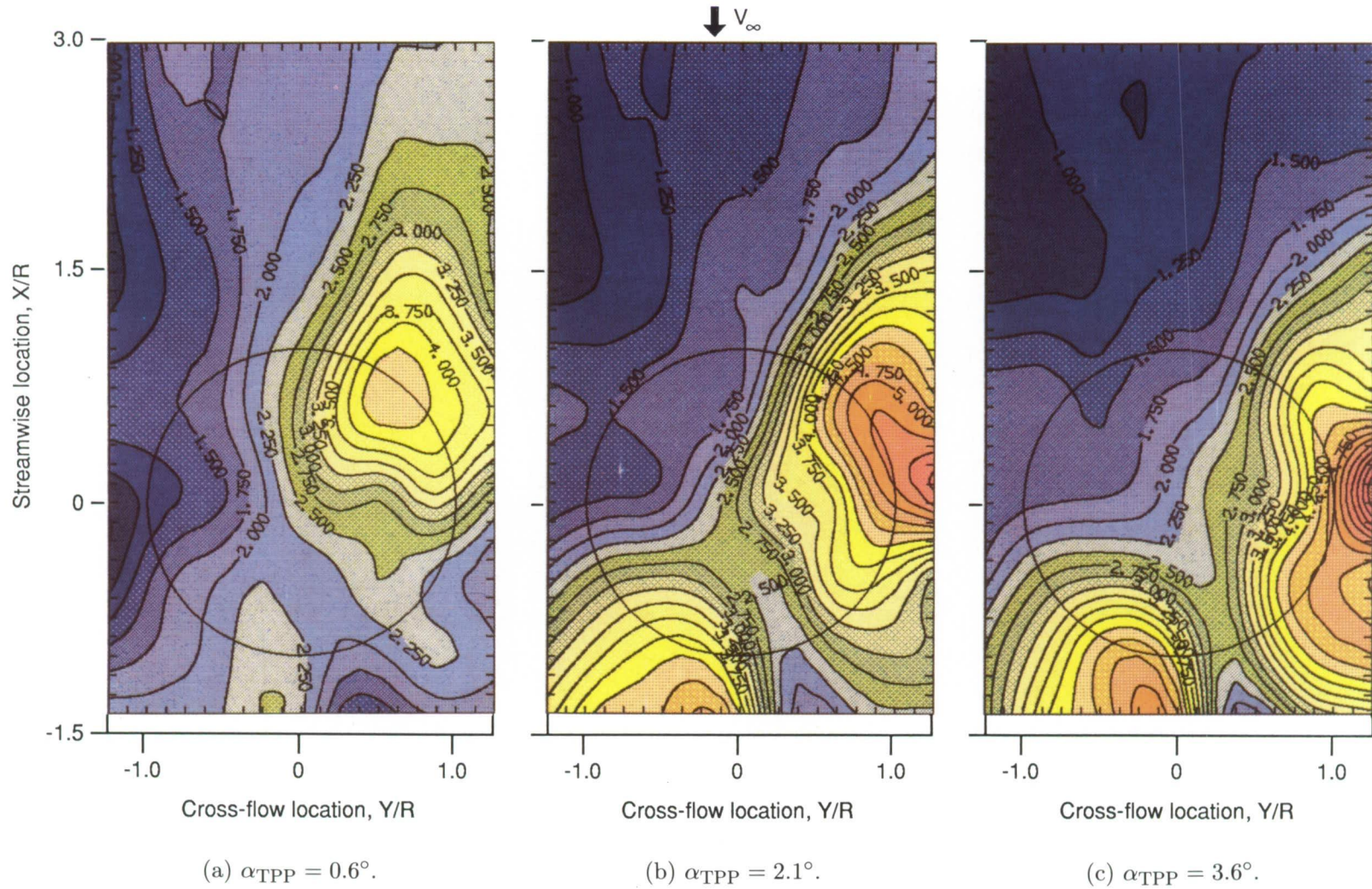


Figure 8. Directivity of rms of filtered time histories (normalized for spherical spreading as shown in fig. 4), $P_{\text{rms}}N$, for $\mu = 0.150$.

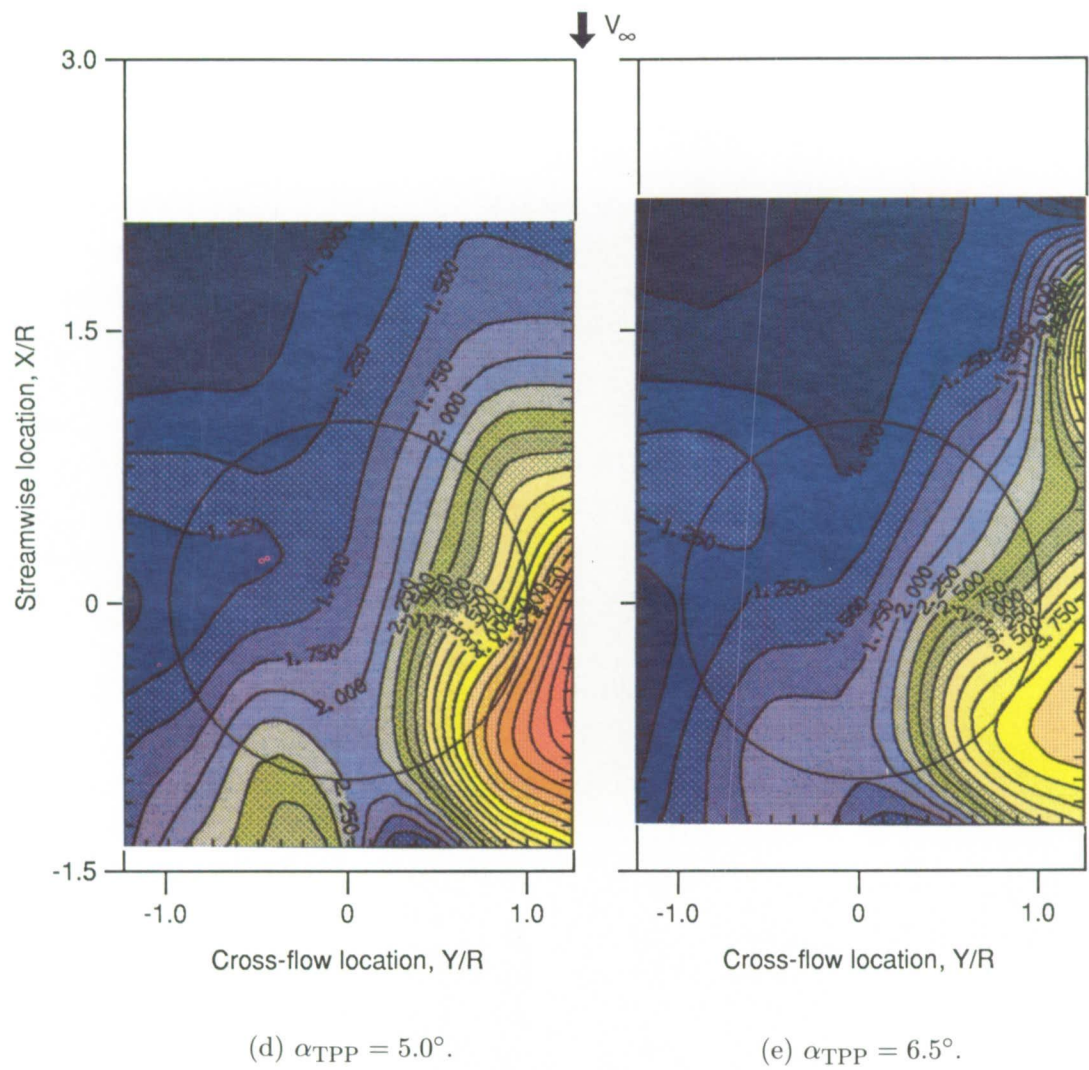


Figure 8. Concluded.

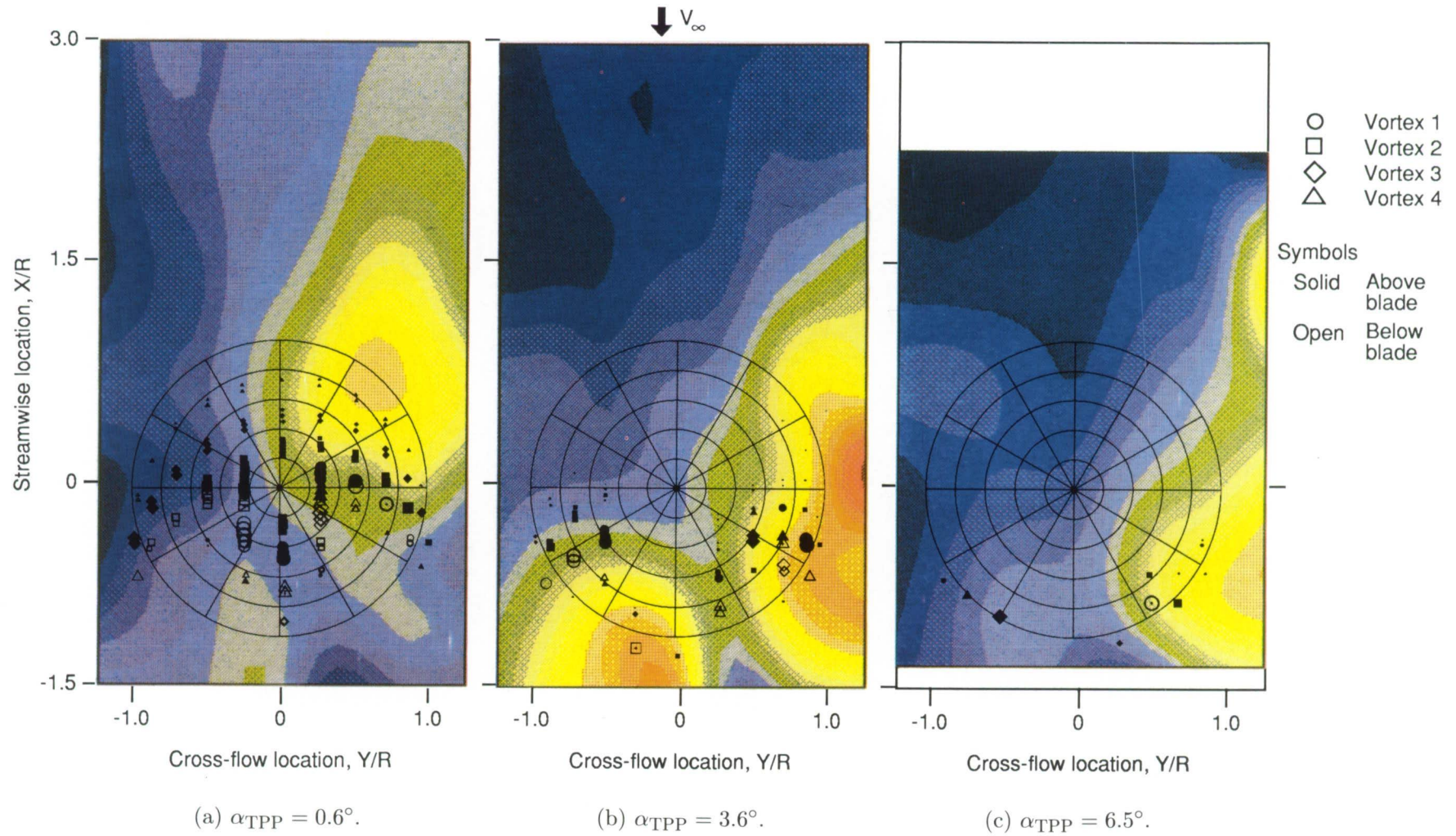
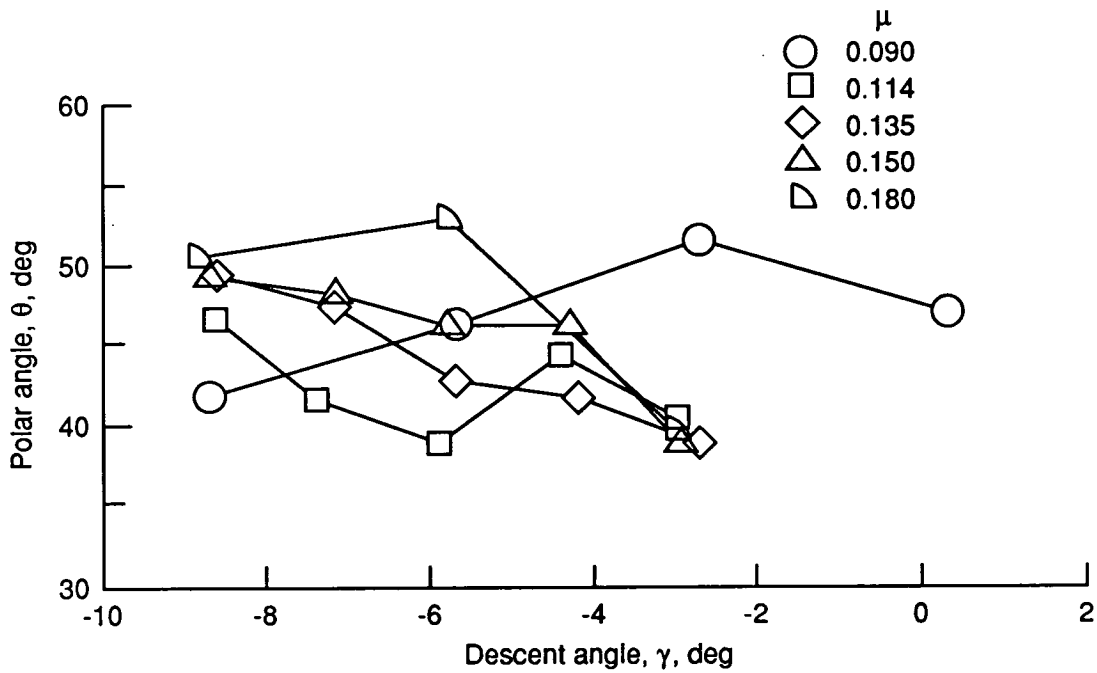
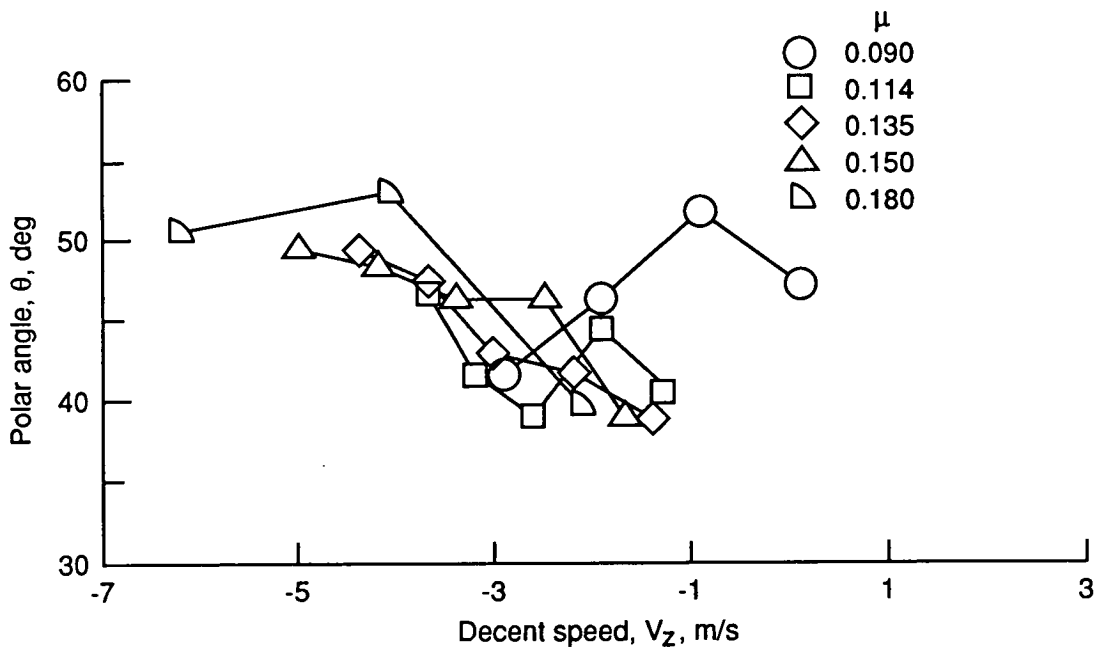


Figure 9. Potential BVI locations from CAMRAD/JA free wake with selected noise directivity patterns of figure 8, $\mu = 0.150$. (Refer to fig. 8 for exact values of contour levels.)

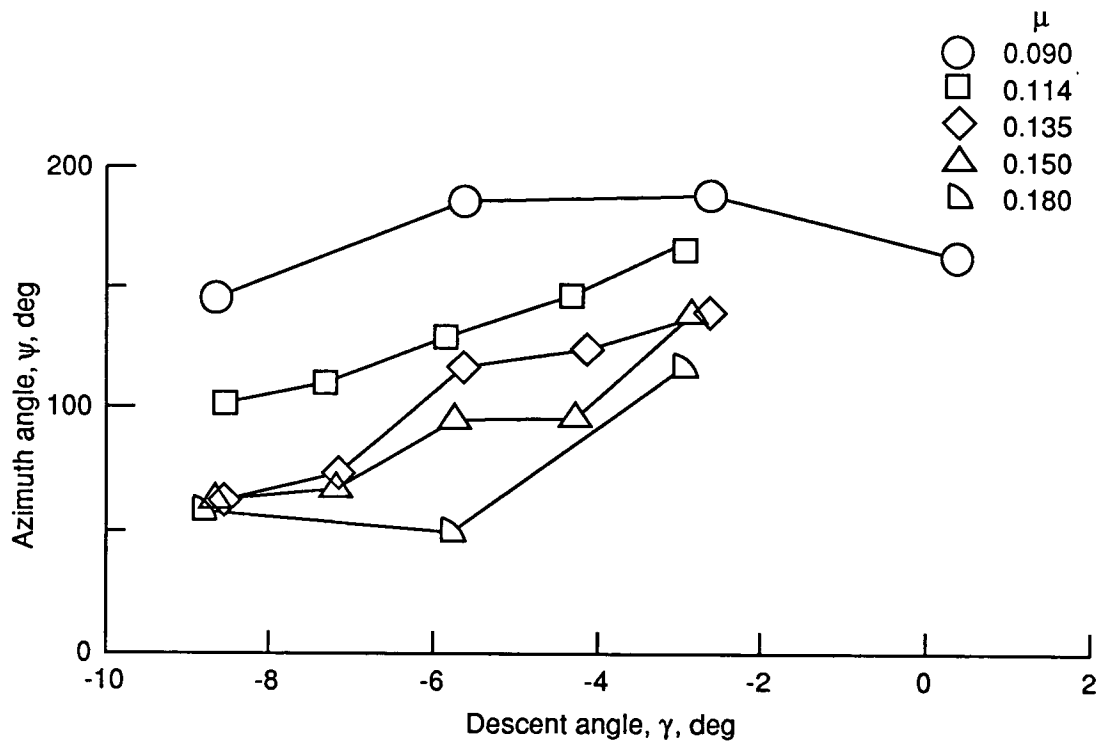


(a) Polar angle versus descent angle.

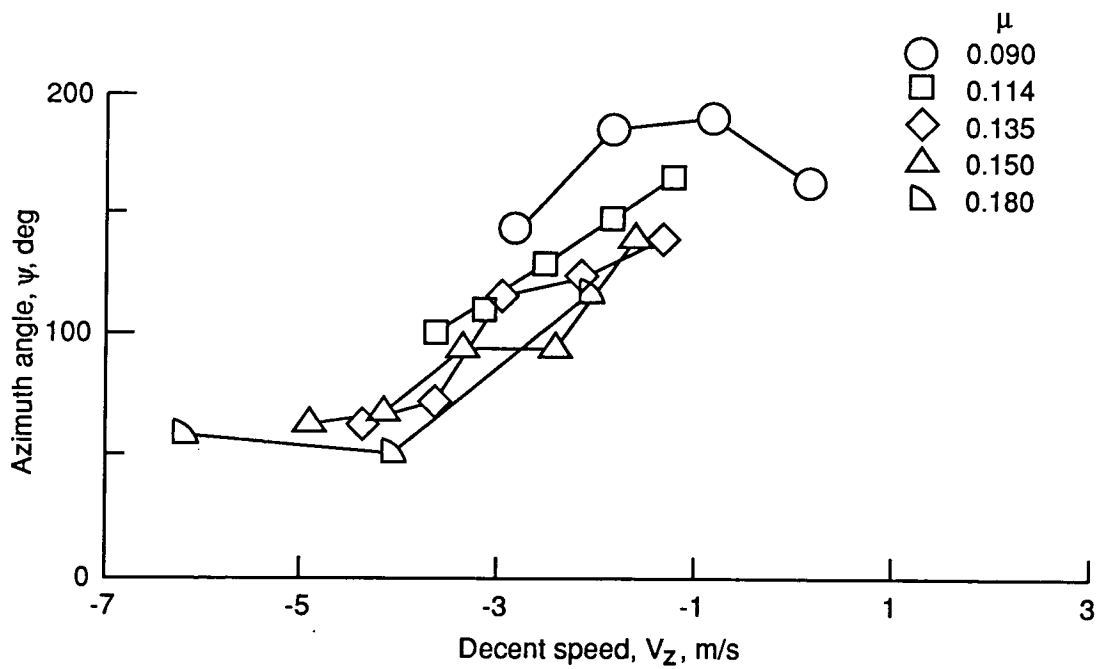


(b) Polar angle versus descent speed.

Figure 10. Variation of polar angle of strongest advancing side BVI radiation with descent condition.



(a) Azimuth angle versus descent angle.



(b) Azimuth angle versus descent speed.

Figure 11. Variation of azimuth angle of strongest advancing side BVI radiation with descent condition.



Report Documentation Page

1. Report No. NASA TP-3015	2. Government Accession No.	3. Recipient's Catalog No.
4. Title and Subtitle Wake Geometry Effects on Rotor Blade-Vortex Interaction Noise Directivity	5. Report Date November 1990	
	6. Performing Organization Code	
7. Author(s) R. M. Martin, Michael A. Marcolini, W. R. Spletstoesser, and K.-J. Schultz	8. Performing Organization Report No. L-16723	
	10. Work Unit No. 505-63-51-06	
9. Performing Organization Name and Address NASA Langley Research Center Hampton, VA 23665-5225	11. Contract or Grant No.	
	13. Type of Report and Period Covered Technical Paper	
12. Sponsoring Agency Name and Address National Aeronautics and Space Administration Washington, DC 20546-0001	14. Sponsoring Agency Code	
	15. Supplementary Notes R. M. Martin and Michael A. Marcolini: Langley Research Center, Hampton, Virginia. W. R. Spletstoesser and K.-J. Schultz: Deutsche Forschungsanstalt für Luft- und Raumfahrt, Braunschweig, West Germany.	
16. Abstract <p>Acoustic measurements from a model rotor wind-tunnel test are presented which show that the directionality of rotor blade-vortex interaction (BVI) noise is strongly dependent on the rotor advance ratio and disk attitude. A rotor free wake analysis is used to show that the general locus of interactions on the rotor disk is also strongly dependent on advance ratio and disk attitude. A comparison of the changing directionality of the BVI noise with changes in the interaction locations shows that the strongest noise radiation occurs in the direction of motion normal to the blade span at the time of interaction for both advancing and retreating side BVI. For advancing side interactions, the BVI radiation angle down from the tip-path plane appears relatively insensitive to rotor operating condition and is typically between 40° and 55° below the disk. However, the azimuthal radiation direction shows a clear trend with descent speed, moving toward the right of the flight path with increasing descent speed. The movement of the strongest radiation direction is attributed to the movement of the interaction locations on the rotor disk with increasing descent speed.</p>		
17. Key Words (Suggested by Authors(s)) Rotor acoustics Blade-vortex interaction noise Acoustic directivity Rotor wake geometry	18. Distribution Statement Unclassified—Unlimited <div style="text-align: right;">Subject Category 71</div>	
19. Security Classif. (of this report) Unclassified	20. Security Classif. (of this page) Unclassified	21. No. of Pages 23
		22. Price A03